



Asynchronous abrupt warming across Eurasia since the 1980s



Yansong Li^{1,2,3,4,5}, Weili Duan^{1,2,3,4,5} ✉, Zhenzhong Zeng⁶, Shan Zou^{1,2,7}, Xu Wang^{1,2}, Ziyang Zhu^{1,2,3,4,5,8}, Enzhao Zhu^{1,2} & Jiayang Wang^{1,2}

Understanding the spatiotemporal dynamics of temperature change is crucial for addressing global warming, particularly as regional climate systems may have passed critical tipping points. Here, we examine temperature change characteristics and influencing factors across the Eurasia from 1901 to 2022. We identify a significant abrupt temperature increase in the 1980s, revealing asynchronous warming patterns across the continent. Abrupt warming occurred after 1970 at 93.6% of Eurasian grid points, with 78.0% concentrated between 1970 and 1990. This abrupt warming is driven largely by the Atlantic Multidecadal Oscillation (AMO), explaining 58% of the variation. Early warming hotspots appeared on the Mongolian Plateau and Central Asia, spreading outward. The most significant warming occurs in middle and high latitudes. Regional differences in hydrothermal conditions and cloud cover lead to varying warming timings across Eurasia. Additionally, the warming exhibits significant seasonal asymmetry, with winter warming predominantly driving the abrupt temperature increase, accounting for 45% of the variance. This is driven by the dominant positive phase of the Arctic Oscillation (AO) in winter.

The Eurasian continent is the largest continental plate in the world, spanning multiple climate zones from the polar regions to the tropics, and nearly encompassing all types of climate. Its geographical complexity and climate diversity make it a key regulating hub for the global climate system^{1–4}. This region plays a key role in global energy and water cycles through the Westerlies and the Asian monsoon^{5,6}. It also provides freshwater for hundreds of millions of people via glacial meltwater from the Tibetan Plateau, known as the Asian Water Tower^{7–9}. However, its unique geographic and climatic characteristics also make it highly vulnerable, and its climate issues have raised significant concerns. For example, the significant temperature difference between the Arctic warming rate and the mid-latitude arid regions has weakened the stability of the westerly jet stream¹⁰, resulting in reduced precipitation in the Eurasia¹¹, increased frequency of dust storms¹², and accelerating the expansion of desertification^{13,14}. Furthermore, the intensity and frequency of heatwave events have increased nonlinearly, further amplifying the risk of an imbalanced water cycle^{15,16}.

Research has shown that since the Industrial Revolution, the rate of warming across the Eurasian continent has shown significant

spatiotemporal heterogeneity^{17–20}. Over the past four decades, the Arctic region has experienced a warming rate 4 times higher than the global average^{21–23}, whereas mid-latitude areas have frequently encountered extreme cold wave events^{24–27}, leading to a nonlinear warming pattern. This uneven warming has not only exacerbated the vulnerability of ecosystems but also triggered a series of cascading effects through multi-layered interactions^{28–30}. This continental-scale anomaly epitomizes the complex spatiotemporal heterogeneity of global warming that extends beyond greenhouse gas forcing^{31–33}. The rapid warming since the 1970s remains poorly understood, but is linked to factors like the North Atlantic Oscillation (NAO) and Pacific Ocean Oscillation (PDO)^{34,35}. While aerosol effects and ocean-atmosphere interactions partially explain mid-century cooling and post-1970s warming^{36–38}, the mechanisms driving regional disparities, particularly in the Northern Hemisphere's climate amplifier zones, remain inadequately resolved. In this context, recent studies have indicated a shift towards a warmer climate regime over inner East Asia since the early 2000s³⁹. This warming has led to surface air

¹State Key Laboratory of Ecological Safety and Sustainable Development in Arid Lands, Xinjiang Institute of Ecology and Geography, Chinese Academy of Sciences, Urumqi, China. ²University of Chinese Academy of Science, Beijing, China. ³Xinjiang Key Laboratory of Water Cycle and Utilization in Arid Zone, Xinjiang Institute of Ecology and Geography, Chinese Academy of Sciences, Urumqi, China. ⁴Ili Station for Watershed Ecosystem Research, Chinese Academy of Sciences, Xinyuan, China. ⁵Tianshan Snowcover and Avalanche Observation and Research Station of Xinjiang, Chinese Academy of Sciences, Xinyuan, China. ⁶School of Environmental Science and Engineering, Southern University of Science and Technology, Shenzhen, China. ⁷Akesu National Station of Observation and Research for Oasis Agro-ecosystem, Akesu, Xinjiang, China. ⁸Soil Physics (SoPHY), Department of Environment, Ghent University, Ghent, Belgium.

✉ e-mail: duanweili@ms.xjbg.ac.cn

temperatures reaching unprecedented levels. Such trends suggest that the inner East Asia may have crossed a critical tipping point—a threshold at which the regional climate could shift abruptly and irreversibly^{40–42}. This raises a critical question about whether similar tipping points have been triggered at different times across various regions of Eurasia, a subject that warrants focused investigation. Currently, no studies have addressed the specific characteristics and mechanisms underlying these regional variations.

Here, we aimed to investigate the characteristics and mechanisms of spatiotemporally-asynchronous abrupt warming across the Eurasian continent from 1901 to 2022 using reanalysis datasets. We identified abrupt temperature shifts in different regions, analyzed the warming trends and magnitudes before and after these shifts, and examined their spatial heterogeneity. This study focused on elucidating the dominant drivers of these asynchronous warming events and uncovering the underlying mechanisms governing their regional variability. Our findings enhance the current understanding of Eurasian climate dynamics and provide critical insights into the broader global climate system.

Results

Characteristics of abrupt temperature changes in Eurasia

We used the Pettitt test to verify whether an abrupt temperature change occurred in Eurasia from 1901 to 2022. The results showed that the average temperature in Eurasia underwent a statistically significant abrupt change in 1980s ($p < 0.01$). Most temperature changes at grid points in Eurasia occurred abruptly after 1970, representing 93.63% of all grid points. Among them, 78.05% were concentrated in the period from 1970 to 1990. Results of abrupt change tests on the Eurasian temperature time series indicate that the warming trend was relatively modest prior to an abrupt shift. In addition to the CRU data, comparisons with ERA5 and NCEP temperature datasets also suggest that abrupt changes generally emerged across the region in the 1980s. However, the exact timing varied spatially, as indicated by the shaded areas in Fig. 1a and the regional heterogeneity illustrated in Fig. 1b. Both the ERA5 and NCEP datasets show a significant increase in temperature, but ERA5 consistently records higher temperatures than NCEP, diverging further after the year 2000. In addition, we examined abrupt temperature changes within the Eurasian region on a grid-point-by-grid-point basis using an abruptness test. The results showed that the timing of the abrupt temperature changes in different regions of Eurasia was inconsistent, and that an obvious sequence of the timing of abrupt temperature changes existed in different regions. The regions in Eurasia where the earliest abrupt changes occurred were located in the Mongolian Plateau and parts of Central Asia (Fig. 1b). Abrupt temperature change in the center of the Mongolian Plateau occurred between 1960 and 1970, while the earliest

change in Central Asia was observed between 1970 and 1980. In contrast, Europe, south-central Eurasia, eastern Russia, and western Asia experienced relatively later abrupt changes, mostly after 1980. This indicates that abrupt warming began in central Eurasia and occurred later in surrounding regions. As shown by the colors and arrows in Fig. 1b, the earliest center of abrupt temperature change was located between the Mongolian Plateau and Central Asia. From this central region, the abrupt change propagated outward in all directions. This pattern suggests a central-origin propagation of abrupt temperature changes across Eurasia, beginning in the Mongolian Plateau and Central Asia and gradually extending to peripheral regions.

Spatiotemporal differences in Eurasian temperature before and after the abrupt change

From 1901 to 2022, the annual average temperature of Eurasia exhibited a significant difference before and after the abrupt change (Fig. S1). The overall average warming rate for the continent was 0.15 °C/decade, with marked differences before and after an abrupt temperature change. Before the abrupt change, Eurasia experienced a modest warming rate of 0.04 °C/decade (Fig. 2b). In contrast, after the abrupt change, the average warming rate increased sharply to 0.41 °C/decade, more than ten times higher (Fig. 2b). The warming was particularly pronounced in the northern-central parts of Eurasia, including the Mongolian Plateau, northern Russia, and Europe, with some areas experiencing warming rates exceeding 0.5 °C/decade (Fig. 2a). The total temperature increase during 1901–2022 was 2.08 °C on average, but the increase was much more significant after the abrupt temperature change (Fig. 2c, d). The increase in the annual average temperature from 1980 to 2022 is more than 1 times higher than that before the abrupt (Fig. 2d). The highest warming occurred in Central Asia, northern Russia, and western Europe, where the increase exceeded 3 °C, while the south-central regions experienced minimal warming, with increases of less than 1 °C (Fig. 2c). These findings highlight the marked spatial and temporal heterogeneity of warming across Eurasia. The most pronounced post-abrupt warming occurred in the mid- to high-latitude regions, driving much of the continent’s overall temperature increase.

The asymmetric seasonal temperature warming in the Eurasia

Analysis of the temperature increase after the abrupt change revealed a significant temperature increase after the abrupt change in all four seasons in Eurasia (Fig. 3). The highest warming occurred in spring (2.16 °C), and a majority of the region warmed by >2 °C during winter, except for some parts of the south-east where warming was less pronounced (Fig. 3a). The next highest season was winter (Fig. 3d), with average warming of 2.14 °C. Warming was less pronounced in the southern part of Eurasia, and a vast majority of the other regions warmed by >3 °C during spring. In addition,

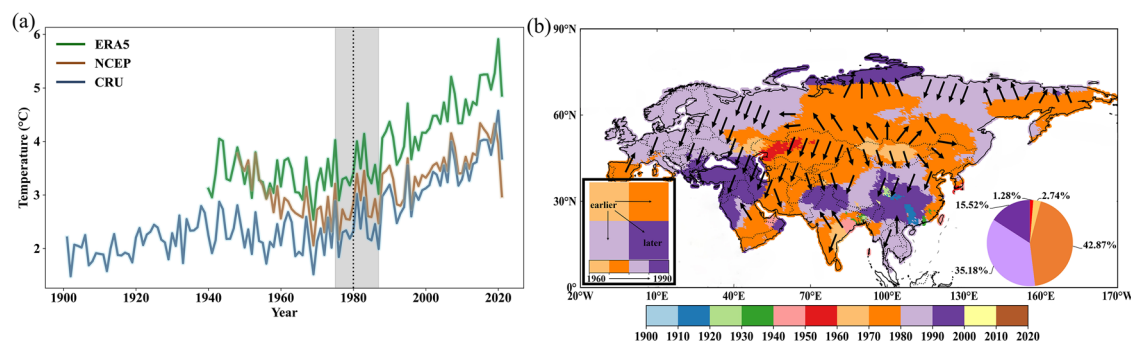


Fig. 1 | Spatiotemporal characteristics of abrupt temperature changes in Eurasia. **a** The abrupt change test of annual mean temperatures on the Eurasian continent from 1901 to 2022. The gray shading represents the overlapping period of the abrupt change points in the annual mean temperatures from the three datasets. The orange dashed line represents the abrupt change time point of the CRU dataset. **b** The abrupt change test results at individual grid points across the Eurasian continent are shown. Different colors represent the timing of abrupt temperature changes in

different periods. Arrows indicate the temporal sequence of these changes: each arrow points from a grid cell where the abrupt change occurred earlier toward an adjacent cell where it occurred later. An illustrative example is provided in the inset (bottom-left), showing one grid point and its neighboring areas. The arrow direction reflects the chronological progression of abrupt temperature changes across the continent. The pie chart in the bottom right corner represents the percentage of time that abrupt temperature changes occurred in the Eurasian continent.

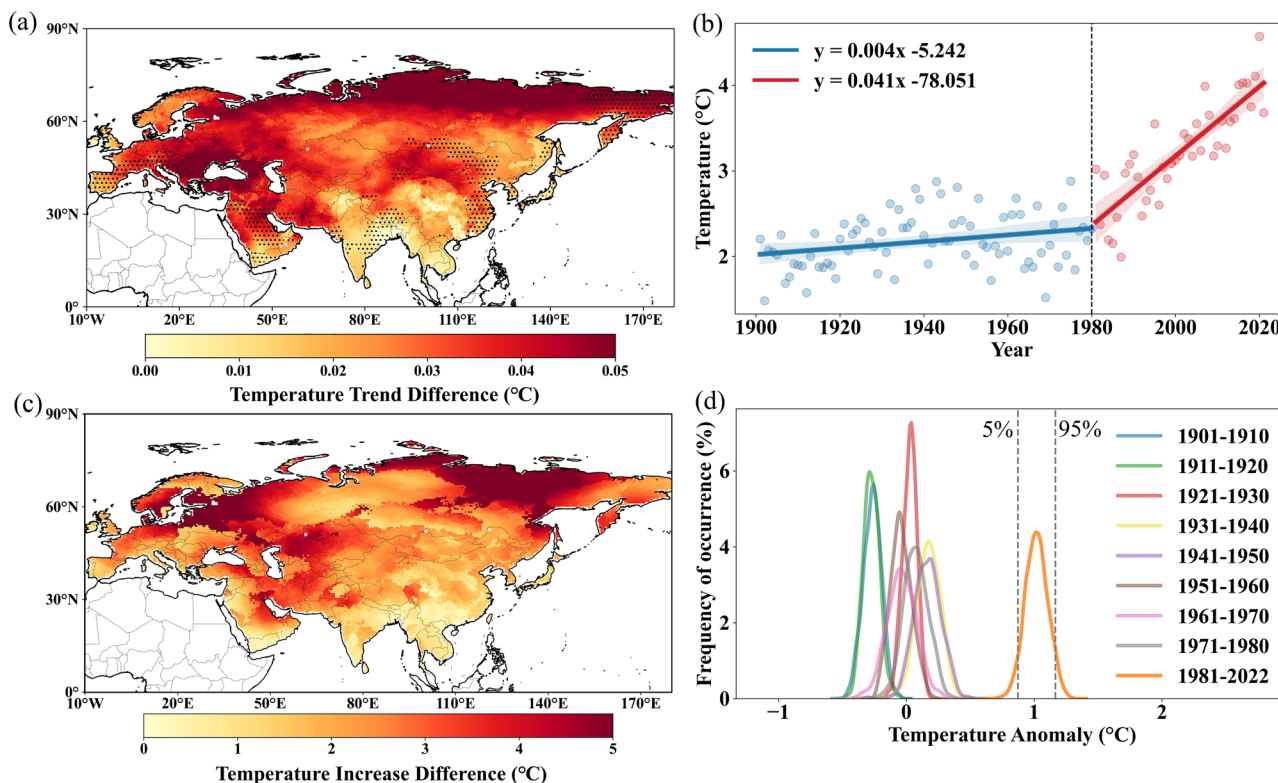


Fig. 2 | Temperature difference patterns in Eurasia before and after the abrupt change. **a** The trend difference of the temperature at each grid point in Eurasia after the abrupt change compared to before the change. Black dots represent significance at the $p < 0.05$ level. **b** Comparison of the annual average temperature regression trends before and after the abrupt change. The blue dots represent the regression scatter points of the annual average temperature from 1901 to 1980, and the blue

dashed line indicates the regression trend. The red dots represent the regression scatter points of the annual average temperature from 1980 to 2022, and the red dashed line indicates the regression trend. **c** The temperature increase difference at each grid point in Eurasia after the abrupt change compared to before the change. **d** Frequency distributions of the mean temperature anomalies (relative to the 1950–1980 mean) over the Eurasia for different time periods from 1901 to 2022.

warming in autumn and summer was less pronounced than in winter and spring, with average temperature increases of 2.09 °C and 1.62 °C, respectively (Fig. 3b, c). Regions with stronger warming during these two seasons were also concentrated in Central Asia, Europe, and the north-central region of Eurasia. The strongest warming in Eurasia occurred in winter and spring, and regions with the highest temperature increases were also concentrated in Central Asia, Europe, and north-central Eurasia. In summary, these regions contributed the most to warming in Eurasia, and warming was mainly concentrated in winter and spring. To determine which season dominates the abrupt warming in the Eurasian continent, we applied the temperature difference decomposition-normalized weight method to calculate the contribution rate of each season. The results show that winter warming is the primary driver of the abrupt temperature increase in Eurasia, with a contribution rate of 45% (Fig. 3d).

Influence of climate mode on temperature

Several previous studies have shown that atmospheric circulation plays a key role in regional climate by transporting heat and moisture between land and sea, and by significantly influencing temperatures in major regions^{35,43,44}. To identify which atmospheric circulation patterns had the strongest influence on Eurasian temperatures—particularly the significant abrupt warming around the 1980s—we analyzed the correlations between 22 major atmospheric circulation indices and regional temperatures across Eurasia (Supplementary Table 1 and Note 1). Pearson correlation analyses showed that the Atlantic Multidecadal Oscillation (AMO, $R = 0.76, p < 0.01$) and Indian Ocean Dipole (IOD, $R = 0.72, p < 0.01$) over 122 years from 1901 to 2022 were strongly correlated. Significant positive correlations ($p < 0.01$) were noted between temperature and the AMO and the IOD (Fig. 4a, c) over almost the entire Eurasian continent. Pearson correlation coefficients of

temperatures with these two circulation factors in the Mongolian Plateau and Central Asia, where the temperature increased early, were >0.7 ($p < 0.01$).

To avoid overfitting, we used a stepwise regression method to identify the most important factors affecting temperature in Eurasia, and the model was set at a 0.05 significance level. We included AMO and IOD data in the regression model, as they showed the highest correlations with temperature across Eurasia. The two indices explained 58% and 4% of the temperature variation, respectively. These results indicate that the AMO was the most dominant factor influencing temperature change in Eurasia, followed by the IOD; however, its explanation rate was much lower than that of AMO. Figure 4b presents the time series of observed Eurasian temperatures and those simulated by a stepwise regression model based on the AMO and IOD from 1901 to 2022. The simulated temperatures closely tracked the CRU observations, highlighting the significant influence of AMO and IOD on temperature variability in Eurasia.

Finally, we trained a binary linear regression model using the time series of the AMO, IOD, and temperature in Eurasia, and applied this model to simulate the complete time series of temperature from 1901 to 2022 based on the AMO and IOD. The results showed that the simulated values of the model accurately reproduced the temperature variations in Eurasia, and the correlation between simulated and actual temperatures was significant ($R = 0.81, p < 0.001$) (Fig. 4d). These results further support a solid causal relationship between the AMO and IOD and temperature changes in Eurasia. However, due to the low explanatory power of IOD in the stepwise regression model, we ultimately concluded that AMO is the most critical factor influencing the temperature in Eurasia. To further test the robustness of our findings, we analyzed simulations from the CESM Large Ensemble (CESM-LE). The analysis revealed a consistent and statistically significant positive correlation between surface temperature over Eurasia and the AMO

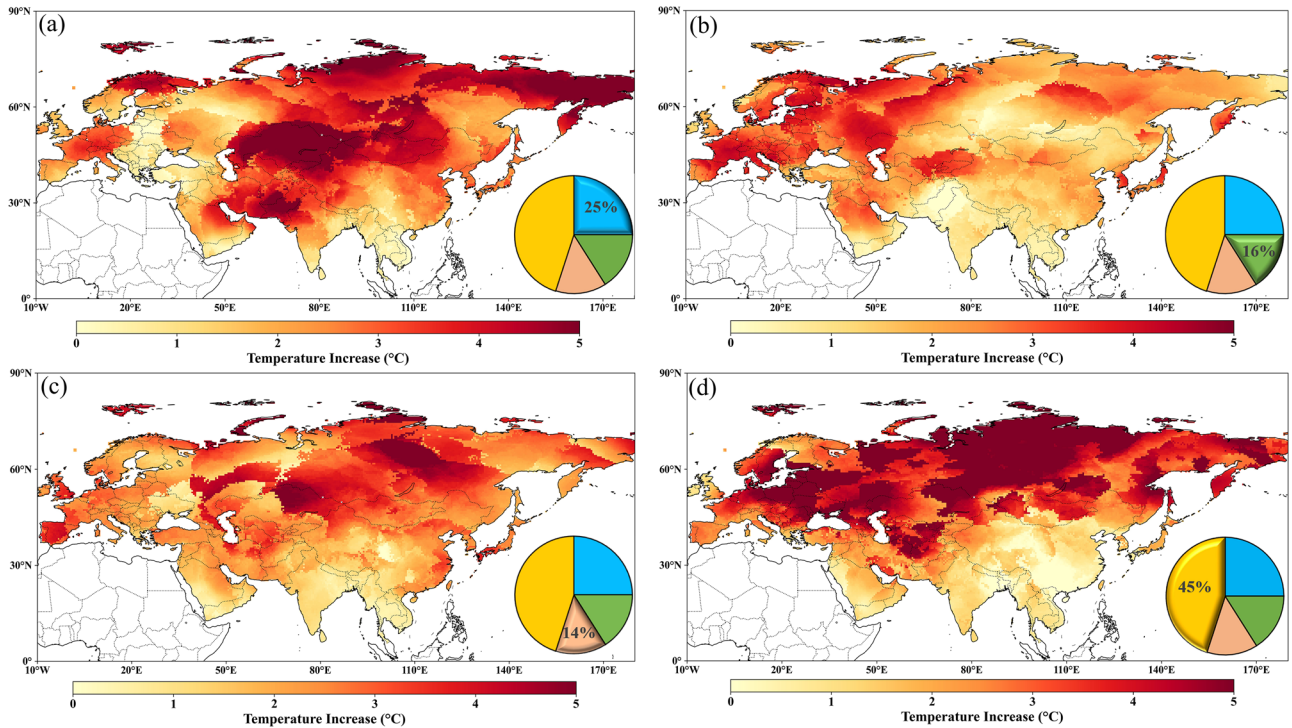


Fig. 3 | Spatial characteristics of temperature increase in four seasons following an abrupt temperature change in Eurasia. Magnitude of temperature increase at grid points across Eurasia during spring (a), summer (b), autumn (c), and winter (d), from the abrupt change point to 2022. The pie charts in the bottom right corners of

the four graphs (a–d) represent the contribution rate of the corresponding seasons to the overall abrupt warming. The blue, green, brown, and yellow colors in the pie chart correspond to spring, summer, autumn, and winter, respectively.

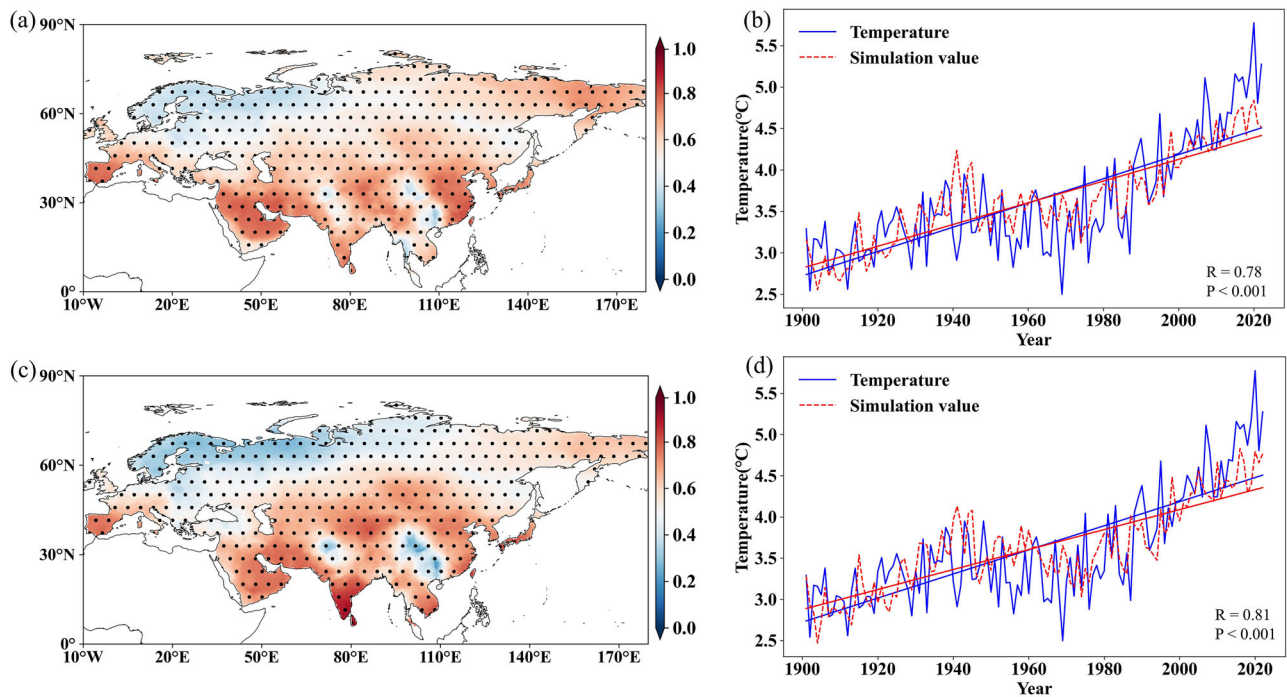


Fig. 4 | Spatiotemporal patterns of temperature and atmospheric circulation. a Spatial pattern of correlation between temperatures on the Eurasian continent and the Atlantic Multidecadal Oscillation (AMO) from 1901 to 2022. Black dots represent significance at $p < 0.05$. b Temporal pattern of Eurasian continental temperatures and temperatures simulated by stepwise regression model based on the

AMO and Indian Ocean Dipole (IOD). c Spatial correlation pattern between temperatures on the Eurasian continent and the IOD from 1901 to 2022. Black dots represent significance at $p < 0.05$. d Temporal pattern of temperatures on the Eurasian continent after the abrupt change and temperatures simulated by a binary linear regression model based on the AMO and IOD.

index, with an ensemble-mean correlation coefficient of 0.57 (Fig. S2). This supports the hypothesis that the AMO plays a primary role in modulating abrupt warming events in the region.

Causes of asynchronous temperature increases in Eurasia

Enhancement of the AMO dominated the abrupt change in mean temperature in Eurasia in 1980s. However, a clear sequence in the timing of abrupt temperature changes existed in regions within Eurasia, and significant differences in temperature increases were noted in different regions and seasons. This was influenced by different factors and cannot be explained by changes in a single element. The region where the abrupt warming first occurred was located in the Mongolian Plateau and Central Asia. First, the relatively small heat capacity of this region, with relatively low soil and atmospheric moisture contents, was an important reason for the first warming in this region (Fig. S3a, b). This change was also due to the enhancement of the AMO since 1980s, which stimulated Rossby wave trains from the Atlantic Ocean to the Eurasian continent. These led to an anomalous high-pressure circulation over the Mongolian Plateau (Fig. 5a, b). This caused significant decrease in cloud cover in this region, and the reduction trend was significantly higher than that in other regions of Eurasia (Fig. 5c). The decrease in cloud cover resulted in a significant increase in solar radiation reaching the surface, leading to the abrupt temperature increase in this region. Moreover, according to the “water-heat coupling”⁴⁵ theory, in areas where the temperature is >0 °C, a decrease in soil moisture will increase temperature (Fig. S3c, d). Soil moisture in Central Asia and the Mongolian Plateau has decreased significantly since 1970, which is also an important reason for the temperature increase in this region (Fig. 5d). In contrast, an abrupt temperature increase in the European region occurred during 1980–1990, slightly later than that in the Mongolian Plateau and Central Asia. According to the linear quasi-geostrophic theoretical framework, surface low pressure balances excess heat by driving cooler subpolar winds towards temperate heat sources through horizontal temperature advection⁴⁶. Thus, the Atlantic Ocean, as a temperate heat source,

was relatively delayed from warming in western Europe owing to cooler subpolar winds balancing some of the heat. In addition, western Europe is a typical temperate oceanic climate zone, and receives more precipitation throughout the year, which dampens warming. Therefore, the combination of these two factors led to a relatively late warming period in the European region. In the Mediterranean region, abrupt warming occurred later, approximately during the 1990–2000 period. This is because winter and spring contributed most to the warming in Eurasia, and the region in question belongs to the Mediterranean climate zone. This climatic pattern coincides with a period of high precipitation, which helps to moderate the warming trend in the region. Furthermore, the increase in cloudiness in the region also contrasted with the decrease in cloudiness in central Eurasia and Europe (Fig. 5c), leading to a weakening of solar radiation reaching the surface of the region and having a dampening effect on warming. The combination of increased cloudiness and precipitation generally delayed warming in the region.

The reasons for the abrupt warming dominated by winter

To explore the reasons why winter warming dominates the abrupt warming in the Eurasian continent, we analyzed the variability of the Arctic Oscillation (AO), a phenomenon closely linked to temperatures in the Northern Hemisphere. Our analysis revealed that from 1950 to 2023, the decadal moving average of the AO exhibited a clear alternation between positive and negative phases. The negative phase dominated before 1975; after that, the positive phase prevailed (Fig. S4). To investigate how changes in the AO phase affect winter temperatures, we analyzed the spatial patterns of global winter wind and temperature anomalies during both positive and negative AO phases. The results showed that during the positive AO phase, surface pressure in the Arctic was lower, and the polar vortex was more compact, restricting cold air to the polar region. At the same time, the westerly jet stream was stronger, and zonal circulation prevailed in mid-latitudes, preventing cold air from invading lower latitudes, resulting in relatively warmer winter temperatures across Eurasia (Fig. 6a, b). In contrast, during the

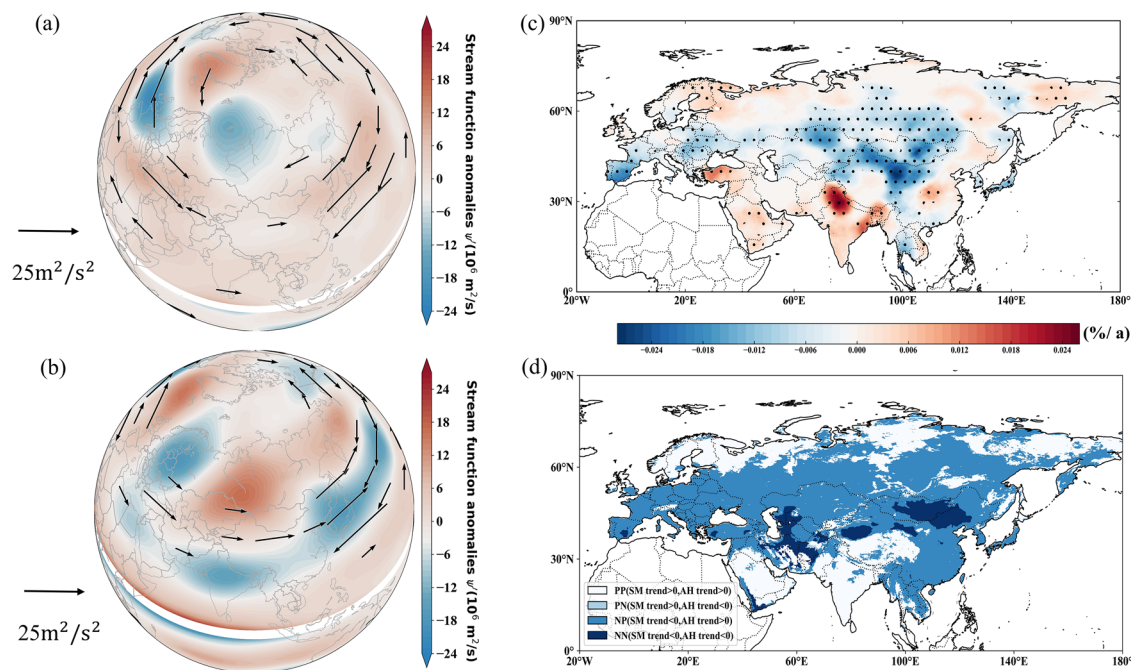


Fig. 5 | Drivers of temperature change across atmospheric and land surface processes. a During the AMO positive phase, spatial patterns of the energy propagation direction of the Rossby wave (black arrows) and the anomalous intensity of high/low pressure systems (shading) at 300 hPa. **b** During the AMO negative phase, spatial patterns of the energy propagation direction of the Rossby wave (black arrows) and the anomalous intensity of high/low pressure systems

(shading) at 300 hPa. **c** Spatial characterization of cloud trends. The black dot areas indicate significant temporal trends ($p < 0.01$). **d** SM and AH trends. Areas with SM trends >0 and AH trends >0 are referred to as PP areas; areas with SM trends >0 and AH trends <0 are called PN areas; areas with SM trends <0 and AH trends >0 are referred to as NP areas, and; areas with SM trends <0 and AH trends <0 are called NN areas.

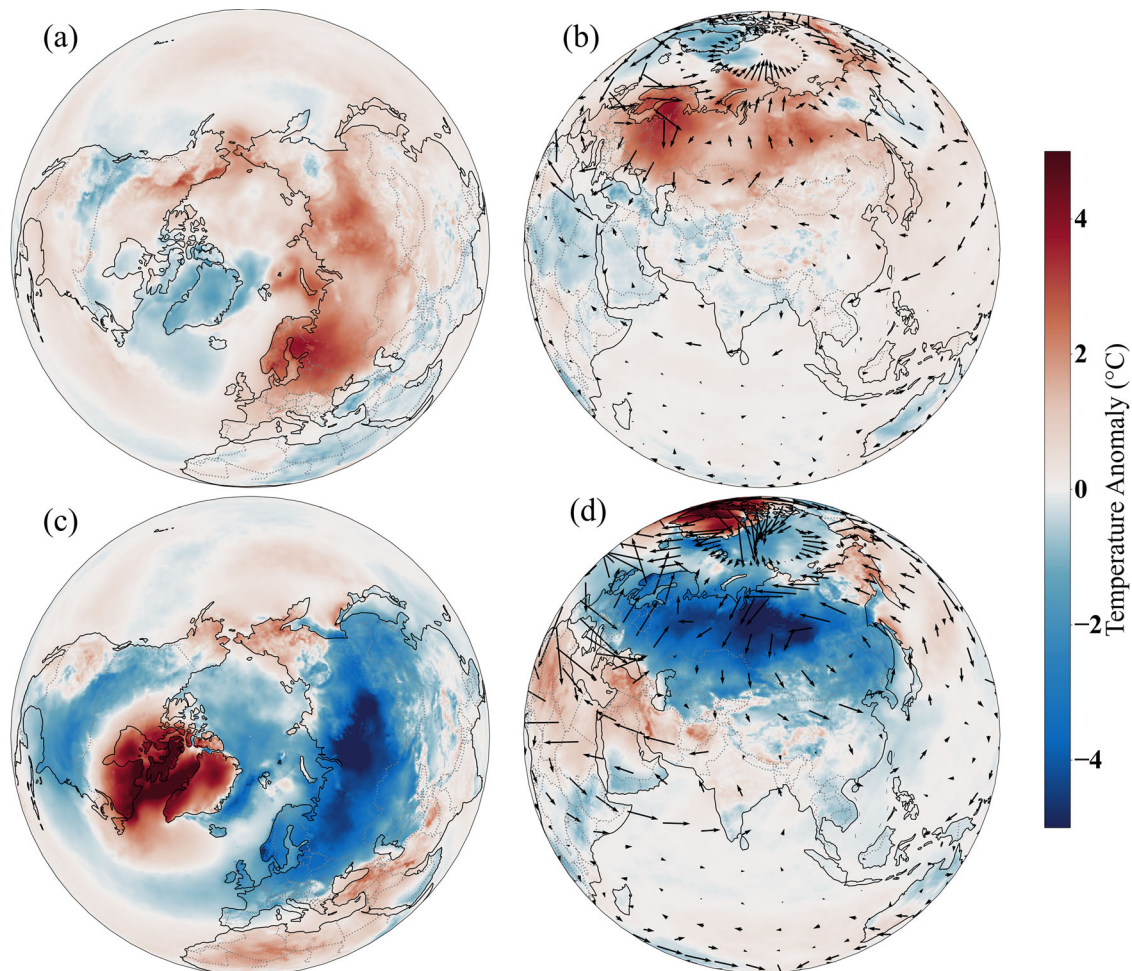


Fig. 6 | Mechanisms for the variations in winter temperature. **a** Spatial patterns of the positive phase of the Arctic Oscillation (AO). **b** Spatial patterns of the wind field (black arrows) anomaly at 500 hPa and temperature anomaly (shading) with the AO-positive phase. **c** Spatial patterns of the AO-negative phase. **d** Spatial patterns of the wind field (black arrows) anomaly at 500 hPa and temperature anomaly (shading) with the AO-negative phase.

negative AO phase, the Arctic high-pressure system strengthened, the pressure gradient weakened, and the polar vortex either split or weakened. This led to a reduction in the strength of the westerly jet stream and an intensification of meridional circulation, allowing cold Arctic air to surge southward into Eurasia, causing lower-than-average winter temperatures across much of the continent (Fig. 6c, d). To avoid bias from a single dataset, we also compared multiple datasets, including CRU, NCEP, and NOAA. The results were completely consistent with ERA5. A positive phase of the AO in winter corresponds to higher temperatures over the Eurasian continent, while a negative phase of the AO in winter corresponds to lower temperatures over the Eurasian continent (Fig. S5). In summary, the positive phase of the AO has dominated over the past 40 years. Its strengthening trend has contributed to rising winter temperatures across Eurasia. This has led to abrupt warming mainly driven by wintertime changes.

Discussion

This study used a temperature dataset from the CRU and atmospheric reanalysis data. It focused on the temperature change in Eurasia from 1901 to 2022, including temperature trends and increases as well as spatial and temporal characteristics of abrupt changes. We found that the temperature change trend and increase in Eurasia have had pronounced spatiotemporal variability. The upward warming trend and increase in temperature have been theoretical over the last 40 years, with an exponential increase in the trend and amplitude, which is more consistent with the results of previous studies related to global temperature change^{47–50}. This suggests that the recent temperature increase is driven by both internal variability within the

Earth system and external forcings. It indicates an irreversible warming mechanism resulting from the combined effects of natural variability and anthropogenic influences^{51,52}.

However, relevant studies on changes in Eurasian temperatures and their influencing factors are limited. Although global warming is primarily driven by greenhouse gas forcing⁵³, the warming patterns are influenced by both external forcing and internal variability, with the timing of regional warming modulated by internal variability. This study identified the AMO as a key atmospheric circulation factor affecting extensive Eurasian temperatures by analyzing major atmospheric circulation factors. The warming trend and temperature increase in Eurasia also exhibited significant spatial variability. The strongest warming was mainly concentrated in Central Asia and the Mongolian Plateau, likely due to the region's unique geographic location and surface characteristics⁵⁴. These regions are located in arid and semi-arid zones, characterized by sparse vegetation and surfaces largely covered by rock and gravel⁵⁵. Rising temperatures have further dried sandy soils and rocks, which increases surface albedo and enhances the reflection of solar radiation back into space⁵⁶. Therefore, the region's surface albedo, desertification, and geophysical feedback mechanisms may have contributed to the observed warming. The magnitude of this warming was significantly higher than in neighboring areas⁵⁷. In addition, the primary characteristic distinguishing arid and semi-arid regions from humid areas is relatively low precipitation. Consequently, these regions lack moisture-bearing air currents that can provide cooling, leading to

more rapid temperature increases^{58,59}. It has also been shown that elevation is an important factor influencing temperature change, and that warming is dependent on elevation in most mountainous regions⁶⁰. In addition, recent studies have found that Arctic amplification and reduction in Arctic sea ice may also affect regional and global temperature changes⁶¹. It has also been suggested that temperature changes in Central Asia are influenced by land-use change⁶², which are directly related to expansion of irrigated agriculture and urbanization in Central Asia⁶³.

Previous studies have shown that aerosol forcing and emissions of greenhouse gases (e.g., CO₂) are important contributors to significant global temperature changes^{32,64,65} and that continued greenhouse gas emissions can lead to continued temperature increases. Large volcanic eruptions can also significantly affect regional and global temperatures³⁷. However, none of these factors cause regional and global temperatures to increase abruptly. A recent study showed that warming of the Mongolian Plateau could not be fully explained by an increase in the intensity of anthropogenic CO₂ emissions. A pacemaker model experiment further supported this conclusion, showing that the dramatic warming over the Mongolian Plateau was driven by an enhanced atmospheric circulation. As a result, the region experienced a sustained increase in surface temperature⁴⁰. Sustained warming, in turn, strengthens the positive terrestrial air feedback and further contributes to an increase in regional temperature^{66,67}, which is in line with our findings. Furthermore, previous study⁶⁸ analyzing multiple meteorological reanalysis datasets found a significant poleward expansion of the Hadley circulation since the 1970s, exceeding 4.5° latitude. This poleward shift in the subtropical descending zone led to increased drought frequency in mid-latitudes of the Northern Hemisphere. This phenomenon is a critical factor contributing to increasing temperatures and may explain the poleward progression of the temperature patterns⁶⁸. Moreover, strengthening of westerly winds north of 45°N in East Asia enhances zonal circulation and suppresses meridional circulation, thereby reducing the southward transport of cold air. In contrast, weakened westerlies at lower latitudes promote meridional circulation and northward transport of warm air, contributing to the latitudinal gradient in temperature increase. This is an important

reason why the temperature increase exhibits characteristic latitudinal evolution⁶⁹.

In this study, we analyzed temperature changes in Eurasia from the twentieth century to date. The asynchronous characteristic of warming was well characterized by the abruptness test. The mechanisms of successive warming in the arid, alpine, humid, and Mediterranean regions of the Eurasian continent were distinctly different. The Mongolian Plateau and Central Asia, which are located in the arid zone of Eurasia, were the first regions to experience abrupt warming. In addition, this region is typical of other arid zones, which have a smaller heat capacity and may also be characterized by a lower heat capacity. A lower heat capacity may also influence earlier and higher warming trends in this region⁷⁰. Immediately following this was abrupt warming in the European region, a phenomenon that was also due to inter-decadal variability in the Atlantic Ocean. North Atlantic positive heat flux anomalies triggered a surface ramp pressure response to diabatic heating, creating the North Atlantic-European West-East (NEW) mode, which led to warming in Europe in a form similar to atmospheric blockage⁷¹. An abrupt temperature change in the Mediterranean region of southeastern Europe occurred significantly later, mainly due to differences in the spatial and temporal precipitation characteristics. During the overall warming in winter and spring over most of Eurasia, increased precipitation in the Mediterranean region had a cooling effect and delayed warming. In contrast, although the difference in the timing of the abrupt temperature increase between the highly mountainous regions of Asia and eastern China was not large, the causes differed. The late onset of abrupt warming in the high Asian mountains was due to localized cooling and drying caused by the Himalayan glaciers⁷². The delayed warming in eastern China can be attributed to the southward displacement of East Asian anticyclonic activity beginning in the 1980s. This shift led to a weakening of the Siberian High in the west and its expansion toward the southeast. Consequently, the intrusion of extremely cold air masses from the north was reduced, contributing to regional warming⁶⁹. Therefore, differences in warming mechanisms across regions can lead to variations in the timing of abrupt warming events. A schematic of mechanisms in different regions is shown in Fig. 7.

The abrupt Eurasian warming since the 1980s is characterized by a high degree of complexity arising from the intricate interactions

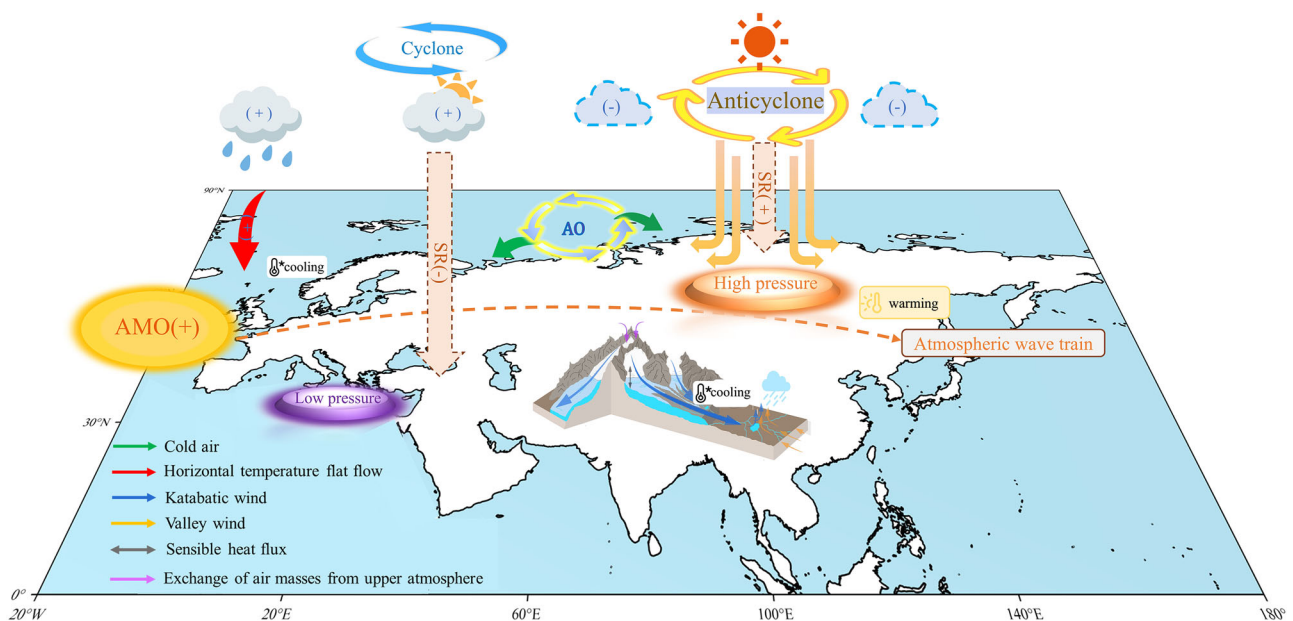


Fig. 7 | Warming mechanisms in different regions of the Eurasian continent. The figure illustrates the AMO-driven abrupt temperature changes over Eurasia since 1980, highlighting regional and seasonal differences in warming timing and mechanisms. Earliest and most pronounced warming occurred over the Mongolian

Plateau and Central Asia due to lower heat capacity, reduced cloud cover, and decreased soil moisture. Europe experienced delayed warming influenced by oceanic moderation and cold advection, while the Mediterranean's warming was further slowed by increased precipitation and cloudiness.

between various climate modes and the precise timing of their phase shifts. AMO and the AO are key players, but their influence is not independent or static^{73,74}. For example, the AMO can modulate the AO's Pacific center intensity (PCI) via the stratospheric polar vortex (SPV). A negative AMO phase tends to strengthen the SPV, which in turn can lead to a more pronounced PCI, thereby altering the spatial expression and impact of the AO^{75,76}. This means that the effect of an AO positive phase on Eurasian temperatures can be amplified or modulated depending on the concurrent phase of the AMO⁷⁷. However, regions experiencing earlier warming were primarily located in arid and semi-arid areas. The temperature increase also exhibited a distinct latitudinal evolution. These patterns may be associated with the unique subsurface properties across climatic zones⁷⁸ and the specific land-atmosphere feedback processes characteristic of arid regions⁷⁹. In addition, the unique features of the water-heat balance and characteristics of energy fluxes in arid zones may influence the regular spatial warming evolution⁸⁰. A series of changes in cloudiness and solar radiation may cause warming of arid zones. Furthermore, the unique water-heat balance and energy flux characteristics of arid zones may also play a key role in shaping the seemingly regular spatial warming patterns^{13,80}. This suggests the need for further in-depth analysis of the underlying mechanisms, particularly from the perspectives of atmospheric physics and hydrology.

Methods

Mann-Kendall trend test

The Mann-Kendall trend test (M-K test) was used to analyze the temporal and spatial temperature trends in Eurasia. The M-K test is a non-parametric statistical method primarily used to detect the presence of monotonic trends in time-series data without requiring the data to obey any particular distribution. The M-K trend test calculates the statistic S to determine the direction and significance of a trend in a time series^{81,82}. The key steps of the method are as follows⁸³: for a given time-series dataset $\{x_1, x_2, \dots, x_n\}$, the difference between each pair of data points in the series is first calculated, and S is calculated using the following formula:

$$S = \sum_{i=1}^{n-1} \sum_{j=i+1}^n \text{sgn}(x_j - x_i). \tag{1}$$

The distribution of S is close to normal; therefore, the standardized statistic Z can be further calculated to assess the significance of the trend:

$$Z = \begin{cases} \frac{S-1}{\sqrt{\text{Var}(S)}}, & S > 0 \\ 0, & S = 0 \\ \frac{S+1}{\sqrt{\text{Var}(S)}}, & S < 0 \end{cases}, \tag{2}$$

where $\text{Var}(S)$ is the variance of S .

In this study, temperature data were used as a time series, and the M-K trend test was applied to calculate S and Z in the time series. The temperature change trend direction (i.e., positive or negative) and the significance level of the trend can be derived from analysis of the Z value. The temperature change trend was considered significant when $|Z|$ was greater than the critical value corresponding to the preset significance level ($\alpha = 0.01$). We define spring as March to May, summer as June to August, autumn as September to November, and winter as December to February.

Pettitt test

The Pettitt test was used to detect mutation points in the temperature time series. The Pettitt test is a non-parametric test commonly used to identify a single mutation point in a time series⁸⁴ and is suitable for use in meteorology, hydrology, and other fields to analyze change points in

a time series⁸⁵. The Pettitt test is based on the Mann-Whitney principle of the rank-sum test, which detects possible mutation points by comparing the differences between the two parts of the sequence before and after detection of possible mutation points. The basic steps are as follows⁸⁶: Given the time-series data of length n $\{x_1, x_2, \dots, x_n\}$, the statistic U_t of the Pettitt test is calculated as follows:

$$U_t = \sum_{i=1}^t \sum_{j=t+1}^n \text{sgn}(x_j - x_i), \tag{3}$$

where t is a potential mutation point in the time series and $\text{sgn}(x_j - x_i)$ is the sign function, which is defined as follows:

$$\text{sgn}(x_j - x_i) = \begin{cases} 1, & x_j > x_i \\ 0, & x_j = x_i \\ -1, & x_j < x_i \end{cases}. \tag{4}$$

The statistic K for the test is defined as:

$$K = \max_{1 \leq t \leq n} |U_t|, \tag{5}$$

where K denotes the most probable mutation point. The significance level of the Pettitt test can be approximated using the following formula:

$$p \approx 2 \exp\left(-\frac{6K^2}{n^3 + n^2}\right). \tag{6}$$

If the calculated p value was less than the preset significance level (0.01), a significant mutation point was considered to exist in the time series.

In this study, temperature time-series data were entered into the Pettitt test to identify abrupt change points in the temperature change process. U_t was first calculated for each possible mutation point, and the maximum statistic K and its corresponding time point were then determined. Significance of the mutation was determined by calculating the p value: if the p value was below a set significance level, the time point was identified as a mutation point in the temperature change.

Stepwise regression models

The specific process of the forward stepwise regression model used in this study was as follows⁸⁷: Starting from the beginning of the model, the independent variables with the smallest p values and those below the significance level were gradually introduced until the p values of all variables to be introduced exceeded a set threshold. In stepwise regression analysis, the basic form of the model is:

$$Y = \beta_0 + \beta_1 X_1 + \beta_2 X_2 + \dots + \beta_k X_k + \epsilon, \tag{7}$$

where Y is the dependent variable (i.e., air temperature in this study); X_1, X_2, \dots, X_k are independent variables (i.e., atmospheric circulation factors in this study); β_0 is the intercept term of the model; $\beta_1, \beta_2, \dots, \beta_k$ are the strengths of the effect of each of the independent variables on the dependent variable, and; ϵ is the error term, which reflects stochastic errors that have not been accounted for by the model.

The goal of stepwise regression is to determine whether the goodness-of-fit (R^2) of the regression model is optimal by gradually introducing or removing independent variables while ensuring simplicity of the model. The significance level (α) was set at 0.05 in this study. Stepwise regression performed t -tests on newly introduced or removed variables at each step; if the p value of a variable was <0.05 , it was considered to have a significant effect on Eurasian air temperature. Conversely, variables with p values >0.05 were removed. This significance level was set to ensure that only variables with statistically significant effects on temperature were included in the model, reducing the possible interference of multicollinearity.

We used the forward stepwise regression algorithm to identify the key climate indices that had the greatest impact on autumn temperature changes from 1901 to 2022, and quantified the contribution of circulation factors to temperature changes. In each step, the values of the p and F statistics were calculated to assess the models that might include predictor variables not supported by the model. For the regression model, we set the significance level at $p < 0.05$. If included in the model, the null hypothesis would have a zero coefficient for the predictor variable. If there was sufficient evidence to reject the null hypothesis (at the given significance level), the predictor variable would be added to the model. The greater the explanatory power of the predictor variable, the earlier it entered the model.

Seasonal contribution analysis

This study employs a contribution rate calculation method based on temperature difference decomposition and normalized weights, aimed at quantifying the relative impact of each season on climate change. First, based on the Pettitt's change point detection method, the study period is divided into a pre-change period ($t_{pre} \in [Y_c - k, Y_c - 1]$) and a post-change period ($t_{post} \in [Y_c + 1, Y_c + k]$), where Y_c is the change year and k is the half-width of the time window (in this study, $k = 20$ years). Next, the temperature difference for each season (spring: March–May, summer: June–August, autumn: September–November, winter: December–February) is calculated before and after the change. The formula for the seasonal temperature difference is as follows:

$$\Delta T_i = \frac{1}{k} \sum_{y=Y_c+1}^{Y_c+k} T_i(y) - \frac{1}{k} \sum_{y=Y_c-k}^{Y_c-1} T_i(y) \quad (8)$$

where $T_i(y)$ is the average temperature of season i in year y ($i = 1, 2, 3, 4$ corresponding to spring, summer, autumn, and winter, respectively), and ΔT_i represents the temperature difference for season i . Then, the contribution rate C_i for season i is defined as the absolute sum of the temperature differences of all seasons divided by the absolute temperature difference of season i , multiplied by 100% to obtain the normalized weight:

$$C_i = \frac{\sum_{j=1}^4 |\Delta T_j|}{|\Delta T_i|} \times 100\% \quad (9)$$

Data availability

The CRU temperature dataset used in this study was CRU TS v.4.07, and the data were downloaded from the official CRU website (<https://crudata.uea.ac.uk/cru/data/hrg/>). Atmospheric circulation factor data selected to resolve the causes of temperature changes were obtained from the Climate Prediction Centre of the National Weather Service (<http://www.cpc.ncep.noaa.gov>). The NCEP temperature data was obtained from the NOAA Physical Sciences Laboratory (<https://psl.noaa.gov/data/gridded/data.ncep.reanalysis.html>). The data used to calculate the Rossby wave fluxes were obtained from the ERA5 reanalysis dataset provided by the European Centre for Medium-Range Weather Forecasts (ECMWF). The variables utilized in this analysis include geopotential, the u-component of wind, and the v-component of wind at the 300 hPa pressure level. Atmospheric humidity and soil moisture data were also downloaded from the ERA5 reanalysis dataset, with a spatial resolution of $0.25^\circ \times 0.25^\circ$ (<https://cds.climate.copernicus.eu/>). The data used to calculate global 500 hPa wind field and temperature anomalies are from ERA5. The NOAA temperature anomaly data were obtained from the National Centers for Environmental Information (NCEI) dataset (<https://www.ncei.noaa.gov/data/>). The Community Earth System Model Large Ensemble Project (CESM2-LE) data are available via <https://www.cesm.ucar.edu/community-projects/lens2/data-sets>. The base map used in this study is the standard map (No. GS(2025)0904) downloaded from the Standard Map Service website of the

National Administration of Surveying, Mapping and Geographic Information of China.

Code availability

The code for this study is available from the corresponding author.

Received: 3 June 2025; Accepted: 18 August 2025;

Published online: 25 September 2025

References

- Li, Q. et al. Different climate response persistence causes warming trend unevenness at continental scales. *Nat. Clim. Chang.* **12**, 343–349 (2022).
- Jiang, J. et al. Spatial patterns of Holocene temperature changes over mid-latitude Eurasia. *Nat. Commun.* **15**, 1507 (2024).
- Ji, K. & Ding, R. Interannual impact of the Victoria mode on the winter-spring surface air temperature over Eurasia and North America. *npj Clim. Atmos. Sci.* **6**, 114 (2023).
- Hu, Y. & Hua, W. Evaluation of summer non-uniform multidecadal temperature variations over Eurasia in CMIP6 models. *JGR Atmos.* **128**, e2023JD039267 (2023).
- Immerzeel, W. W. et al. Importance and vulnerability of the world's water towers. *Nature* **577**, 364–369 (2020).
- Eagle, R. A. et al. High regional climate sensitivity over continental China constrained by glacial-recent changes in temperature and the hydrological cycle. *Proc. Natl. Acad. Sci. USA* **110**, 8813–8818 (2013).
- Kraaijenbrink, P. D. A. et al. Climate change decisive for Asia's snow meltwater supply. *Nat. Clim. Change* **11**, 591–597 (2021).
- Zhang, Q. et al. Oceanic climate changes threaten the sustainability of Asia's water tower. *Nature* **615**, 87–93 (2023).
- Yao, T. et al. The imbalance of the Asian water tower. *Nat. Rev. Earth Environ.* **3**, 618–632 (2022).
- Alizadeh, O. & Lin, Z. Rapid Arctic warming and its link to the waviness and strength of the westerly jet stream over West Asia. *Glob. Planet. Change* **199**, 103447 (2021).
- Routson, C. C. et al. Mid-latitude net precipitation decreased with Arctic warming during the Holocene. *Nature* **568**, 83–87 (2019).
- Ma, Y. et al. Increasing cross-border dust storm from Mongolia to China during 1987–2022. *Glob. Planet. Change* **242**, 104578 (2024).
- Huang, J., Yu, H., Guan, X., Wang, G. & Guo, R. Accelerated dryland expansion under climate change. *Nat. Clim. Change* **6**, 166–171 (2016).
- Koppa, A. et al. Dryland self-expansion enabled by land–atmosphere feedbacks. *Science* **385**, 967–972 (2024).
- Alizadeh, M. R. et al. A century of observations reveals increasing likelihood of continental-scale compound dry-hot extremes. *Sci. Adv.* **6**, eaaz4571 (2020).
- Christidis, N., Jones, G. S. & Stott, P. A. Dramatically increasing chance of extremely hot summers since the 2003 European heatwave. *Nat. Clim. Change* **5**, 46–50 (2015).
- Zhong, Z. et al. Reversed asymmetric warming of sub-diurnal temperature over land during recent decades. *Nat. Commun.* **14**, 7189 (2023).
- Bader, J. et al. Global temperature modes shed light on the Holocene temperature conundrum. *Nat. Commun.* **11**, 4726 (2020).
- Kaufman, D. S. & Broadman, E. Revisiting the Holocene global temperature conundrum. *Nature* **614**, 425–435 (2023).
- Jun, Y.-J. & Son, S.-W. A zonal asymmetry in boreal winter surface temperature trend and its recent reversal over the Northern Hemisphere continents. *npj Clim. Atmos. Sci.* **8**, 65 (2025).
- Rantanen, M. Natural variability boosts Arctic warming. *Nat. Geosci.* **17**, 485–486 (2024).
- Zhou, W., Leung, L. R. & Lu, J. Steady threefold Arctic amplification of externally forced warming masked by natural variability. *Nat. Geosci.* **17**, 508–515 (2024).

23. Rantanen, M. et al. The Arctic has warmed nearly four times faster than the globe since 1979. *Commun. Earth Environ.* **3**, 168 (2022).
24. Cohen, J., Agel, L., Barlow, M. & Entekhabi, D. No detectable trend in mid-latitude cold extremes during the recent period of Arctic amplification. *Commun. Earth Environ.* **4**, 341 (2023).
25. Nakamura, T., Yamazaki, K., Sato, T. & Ukita, J. Memory effects of Eurasian land processes cause enhanced cooling in response to sea ice loss. *Nat. Commun.* **10**, 5111 (2019).
26. Yin, M., Yang, X.-Q., Sun, L., Tao, L. & Keenlyside, N. Amplified wintertime Arctic warming causes Eurasian cooling via nonlinear feedback of suppressed synoptic eddy activities. *Sci. Adv.* **11**, eadr6336 (2025).
27. Gong, H. et al. Teleconnection from Arctic warming suppresses long-term warming in central Eurasia. *Sci. Adv.* **11**, eadq9461 (2025).
28. Su, H. et al. Weakening and strengthening structures in the Hadley Circulation change under global warming and implications for cloud response and climate sensitivity. *JGR Atmos.* **119**, 5787–5805 (2014).
29. Pottier, P. et al. Vulnerability of amphibians to global warming. *Nature* **639**, 954–961 (2025).
30. Yang, H. et al. Onshore intensification of subtropical western boundary currents in a warming climate. *Nat. Clim. Chang.* **15**, 301–307 (2025).
31. Pathirana, G. et al. Increase in convective extreme El Niño events in a CO₂ removal scenario. *Sci. Adv.* **9**, eadh2412 (2023).
32. Li, Z. et al. Aerosol and monsoon climate interactions over Asia. *Rev. Geophys.* **54**, 866–929 (2016).
33. Jones, M. W. et al. National contributions to climate change due to historical emissions of carbon dioxide, methane, and nitrous oxide since 1850. *Sci. Data* **10**, 155 (2023).
34. Delworth, T. L. et al. The North Atlantic Oscillation as a driver of rapid climate change in the Northern Hemisphere. *Nat. Geosci.* **9**, 509–512 (2016).
35. Steinman, B. A., Mann, M. E. & Miller, S. K. Atlantic and Pacific multidecadal oscillations and Northern Hemisphere temperatures. *Science* **347**, 988–991 (2015).
36. Charlson, R. J. et al. Climate forcing by anthropogenic aerosols. *Science* **255**, 423–430 (1992).
37. Thompson, D. W. J., Kennedy, J. J., Wallace, J. M. & Jones, P. D. A large discontinuity in the mid-twentieth century in observed global-mean surface temperature. *Nature* **453**, 646–649 (2008).
38. Thompson, D. W. J., Wallace, J. M., Kennedy, J. J. & Jones, P. D. An abrupt drop in Northern Hemisphere sea surface temperature around 1970. *Nature* **467**, 444–447 (2010).
39. Zhang, P. et al. Abrupt shift to hotter and drier climate over inner East Asia beyond the tipping point. *Science* **370**, 1095–1099 (2020).
40. Cai, Q. et al. Recent pronounced warming on the Mongolian Plateau boosted by internal climate variability. *Nat. Geosci.* **17**, 181–188 (2024).
41. Lenton, T. M. Early warning of climate tipping points. *Nat. Clim. Change* **1**, 201–209 (2011).
42. Lenton, T. M. et al. Climate tipping points—too risky to bet against. *Nature* **575**, 592–595 (2019).
43. Vautard, R. et al. Heat extremes in Western Europe increasing faster than simulated due to atmospheric circulation trends. *Nat. Commun.* **14**, 6803 (2023).
44. Horton, D. E. et al. Contribution of changes in atmospheric circulation patterns to extreme temperature trends. *Nature* **522**, 465–469 (2015).
45. Jiang, K. et al. Combined influence of soil moisture and atmospheric humidity on land surface temperature under different climatic background. *iScience* **26**, 106837 (2023).
46. Klein, R., Schielicke, L., Pfahli, S. & Khouider, B. QG–DL–Ekman: dynamics of a diabatic layer in the quasi-geostrophic framework. *J. Atmos. Sci.* **79**, 887–905 (2022).
47. Baines, P. G. & Folland, C. K. Evidence for a rapid global climate shift across the late 1960s. *J. Clim.* **20**, 2721–2744 (2007).
48. Hansen, J. et al. Global temperature change. *Proc. Natl. Acad. Sci. USA* **103**, 14288–14293 (2006).
49. Jones, P. D., New, M., Parker, D. E., Martin, S. & Rigor, I. G. Surface air temperature and its changes over the past 150 years. *Rev. Geophys.* **37**, 173–199 (1999).
50. Stott, P. A. et al. Observational constraints on past attributable warming and predictions of future global warming. *J. Clim.* **19**, 3055–3069 (2006).
51. Gong, H., Wang, L., Chen, W. & Wu, R. Attribution of the East Asian winter temperature trends during 1979–2018: role of external forcing and internal variability. *Geophys. Res. Lett.* **46**, 10874–10881 (2019).
52. Najafi, M. R., Zwiers, F. W. & Gillett, N. P. Attribution of Arctic temperature change to greenhouse-gas and aerosol influences. *Nat. Clim. Change* **5**, 246–249 (2015).
53. Hansen, J. et al. Climate impact of increasing atmospheric carbon dioxide. *Science* **213**, 957–966 (1981).
54. Charney, J. G. Dynamics of deserts and drought in the Sahel. *Q. J. R. Meteorol. Soc.* **101**, 193–202 (1975).
55. Qiao, L. et al. Soil moisture–atmosphere coupling accelerates global warming. *Nat. Commun.* **14**, 4908 (2023).
56. Zuo, Z. et al. Importance of soil moisture conservation in mitigating climate change. *Sci. Bull.* **69**, 1332–1341 (2024).
57. Perkins, S. Albedo is a simple concept that plays complicated roles in climate and astronomy. *Proc. Natl. Acad. Sci. USA* **116**, 25369–25371 (2019).
58. Huang, J., Guan, X. & Ji, F. Enhanced cold-season warming in semi-arid regions. *Atmos. Chem. Phys.* **12**, 5391–5398 (2012).
59. Li, Y., Ding, Y. & Li, W. Interdecadal variability of the Afro-Asian summer monsoon system. *Adv. Atmos. Sci.* **34**, 833–846 (2017).
60. Mountain Research Initiative EDW Working Group. Elevation-dependent warming in mountain regions of the world. *Nat. Clim. Change* **5**, 424–430 (2015).
61. Dong, J. et al. Arctic sea ice loss warmed the temperate East Asian winter in the mid-Holocene. *Commun. Earth Environ.* **5**, 401 (2024).
62. Lioubimtseva, E. & Cole, R. Uncertainties of climate change in arid environments of Central Asia. *Rev. Fish. Sci.* **14**, 29–49 (2006).
63. Lioubimtseva, E. & Henebry, G. M. Climate and environmental change in arid Central Asia: impacts, vulnerability, and adaptations. *J. Arid Environ.* **73**, 963–977 (2009).
64. Lohmann, U. Why does knowledge of past aerosol forcing matter for future climate change?. *JGR Atmos.* **122**, 5021–5023 (2017).
65. Lashof, D. A. & Ahuja, D. R. Relative contributions of greenhouse gas emissions to global warming. *Nature* **344**, 529–531 (1990).
66. Humphrey, V. et al. Soil moisture–atmosphere feedback dominates land carbon uptake variability. *Nature* **592**, 65–69 (2021).
67. Berg, A. et al. Land–atmosphere feedbacks amplify aridity increase over land under global warming. *Nat. Clim. Change* **6**, 869–874 (2016).
68. Hu, Y. & Fu, Q. Observed poleward expansion of the Hadley circulation since 1979. *Atmos. Chem. Phys.* **7**, 5229–5236 (2007).
69. Zhi, X., Tian, X., Liu, P. & Hu, Y. Interdecadal variations in winter extratropical anticyclones in East Asia and their impacts on the decadal mode of East Asian surface air temperature. *Meteorol. Atmos. Phys.* **131**, 1763–1775 (2019).
70. Ji, F., Wu, Z., Huang, J. & Chassignet, E. P. Evolution of land surface air temperature trend. *Nat. Clim. Change* **4**, 462–466 (2014).
71. Ghosh, R., Müller, W. A., Baehr, J. & Bader, J. Impact of observed North Atlantic multidecadal variations to European summer climate: a linear baroclinic response to surface heating. *Clim. Dyn.* **48**, 3547–3563 (2017).
72. Salerno, F. et al. Local cooling and drying induced by Himalayan glaciers under global warming. *Nat. Geosci.* **16**, 1120–1127 (2023).
73. Jeong, D., Yoo, C. & Yeh, S.-W. Contributions of external forcing and internal variability to the multidecadal warming rate of East Asia in the present and future climate. *npj Clim. Atmos. Sci.* **7**, 22 (2024).

74. Dong, B. & Sutton, R. T. Drivers and mechanisms contributing to excess warming in Europe during recent decades. *npj Clim. Atmos. Sci.* **8**, 41 (2025).
75. Gong, H., Ma, K., Liu, B., Cohen, J. & Wang, L. Structural fluctuations of the Arctic oscillation tied to the Atlantic multidecadal oscillation. *npj Clim. Atmos. Sci.* **7**, 260 (2024).
76. Liu, J., Xue, J., Gao, Y. & Zhu, H. The influence of Arctic oscillation on South China precipitation in winter is modulated by the Atlantic multidecadal oscillation. *Geophys. Res. Lett.* **51**, e2024GL11209 (2024).
77. Fang, M., Li, X., Chen, H. W. & Chen, D. Arctic amplification modulated by Atlantic multidecadal oscillation and greenhouse forcing on multidecadal to century scales. *Nat. Commun.* **13**, 1865 (2022).
78. Li, H.-Y. et al. Study of energy partitioning and its feedback on the microclimate over different surfaces in an arid zone. *Acta Phys. Sin.* **64**, 059201 (2015).
79. Schumacher, D. L., Keune, J. & Dirmeyer, P. Drought self-propagation in drylands due to land-atmosphere feedbacks. *Nat Geosci.* **15**, 262–268 (2022).
80. Huntingford, C. et al. Acceleration of daily land temperature extremes and correlations with surface energy fluxes. *npj. Clim. Atmos. Sci.* **7**, 84 (2024).
81. Mann, H. B. Nonparametric tests against trend. *Econometrica* **13**, 245 (1945).
82. Yue, S., Pilon, P. & Cavadias, G. Power of the Mann–Kendall and Spearman’s rho tests for detecting monotonic trends in hydrological series. *J. Hydrol.* **259**, 254–271 (2002).
83. Asfaw, A., Simane, B., Hassen, A. & Bantider, A. Variability and time series trend analysis of rainfall and temperature in northcentral Ethiopia: a case study in Woleka sub-basin. *Weather Clim. Extremes* **19**, 29–41 (2018).
84. Pettitt, A. N. A non-parametric approach to the change-point problem. *Appl. Stat.* **28**, 126 (1979).
85. Praveen, B. et al. Analyzing trend and forecasting of rainfall changes in India using non-parametrical and machine learning approaches. *Sci. Rep.* **10**, 10342 (2020).
86. Gao, P., Mu, X.-M., Wang, F. & Li, R. Changes in streamflow and sediment discharge and the response to human activities in the middle reaches of the Yellow River. *Hydrol. Earth Syst. Sci.* **15**, 1–10 (2011).
87. Zeng, Z. et al. A reversal in global terrestrial stilling and its implications for wind energy production. *Nat. Clim. Chang.* **9**, 979–985 (2019).

Acknowledgements

This work was supported by the Strategic Priority Research Program of the Chinese Academy of Sciences (Grant No. XDB0720400), the Tianshan Talent Training Program (Grant No. 2023TSYCLJ0050), the West Light Foundation of the Chinese Academy of Sciences (Grant No. xbzg-zdsys-

202208), and the Science Foundation of Xinjiang Institute of Ecology and Geography, Chinese Academy of Sciences (E3500101).

Author contributions

Y.L. wrote the original draft, and contributed to software, methodology, and investigation. W.D. wrote the review & editing, supervised the project, administered the project, conducted formal analysis, and contributed to conceptualization. Z.Ze. supervised and reviewed the manuscript. S.Z. modified, supervised and contributed to conceptualization. X.W. contributed to software and methodology. Z.Zh. contributed to software and methodology. E.Z. contributed to software and methodology. J.W. contributed to software and methodology. All authors reviewed the manuscript.

Competing interests

The authors declare no competing interests.

Additional information

Supplementary information The online version contains supplementary material available at <https://doi.org/10.1038/s41612-025-01209-3>.

Correspondence and requests for materials should be addressed to Weili Duan.

Reprints and permissions information is available at <http://www.nature.com/reprints>

Publisher’s note Springer Nature remains neutral with regard to jurisdictional claims in published maps and institutional affiliations.

Open Access This article is licensed under a Creative Commons Attribution-NonCommercial-NoDerivatives 4.0 International License, which permits any non-commercial use, sharing, distribution and reproduction in any medium or format, as long as you give appropriate credit to the original author(s) and the source, provide a link to the Creative Commons licence, and indicate if you modified the licensed material. You do not have permission under this licence to share adapted material derived from this article or parts of it. The images or other third party material in this article are included in the article’s Creative Commons licence, unless indicated otherwise in a credit line to the material. If material is not included in the article’s Creative Commons licence and your intended use is not permitted by statutory regulation or exceeds the permitted use, you will need to obtain permission directly from the copyright holder. To view a copy of this licence, visit <http://creativecommons.org/licenses/by-nc-nd/4.0/>.

© The Author(s) 2025